ADVANCED ENERGY MATERIALS

Supporting Information

for *Adv. Energy Mater.,* DOI: 10.1002/aenm.202102939

Optimizing the Proton Conductivity with the Isokinetic Temperature in Perovskite-Type Proton Conductors According to Meyer–Neldel Rule

Peng Du, Nana Li, Xiao Ling, Zhijun Fan, Artur Braun, Wenge Yang, Qianli Chen,* and Arthur Yelon*

Supporting Information

Optimizing the proton conductivity with the isokinetic temperature in perovskite-type proton conductors according to Meyer-Neldel Rule

Peng Du[1], Nana Li[2], Xiao Ling[1], Zhijun Fan[1], Artur Braun[3], Wenge Yang[2,*], Qianli Chen[1,*], Arthur Yelon [4]

Peng Du, Dr. Xiao Ling, Zhijun Fan, Prof. Qianli Chen

University of Michigan – Shanghai Jiao Tong University Joint Institute, Shanghai Jiao Tong University, Shanghai, 200240, China

E-mail: qianli.chen@sjtu.edu.cn

Dr. Nana Li, Prof. Wenge Yang

Center for High Pressure Science & Technology Advanced Research (HPSTAR), Shanghai 201203, China

E-mail: yangwg@hpstar.ac.cn

Dr. Artur Braun

Laboratory for High Performance Ceramics, Empa. Swiss Federal Laboratories for Materials Science and Technology, CH-8600 Dübendorf, Switzerland

Prof. Arthur Yelon

Département de Génie Physique, Polytechnique Montréal and Réseau Québecois sur des Matériaux de Pointe (RQMP), CP 6079, Succursale and C-V, Montréal, QC H3C 3A7, Canada

Proton conductivity

Typical impedance spectra for proton conducting perovskites show two semicircles: at high-frequency for grain interior (referred as bulk), and at low-frequency for from grain boundaries.

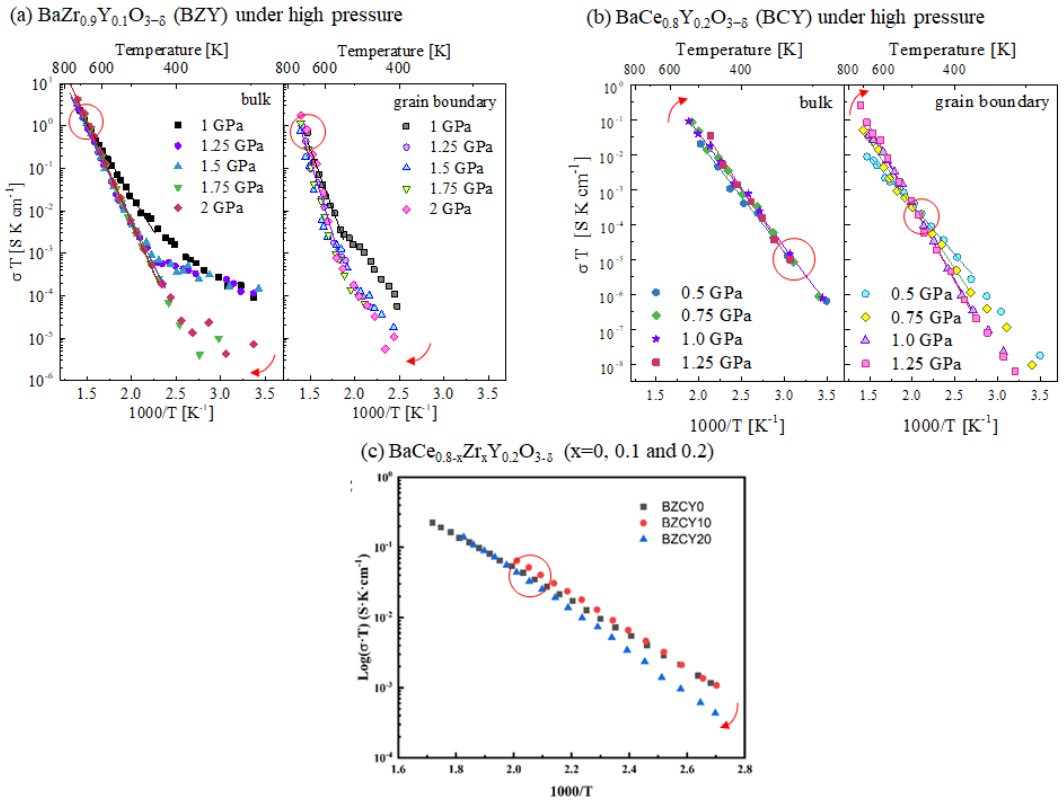

Figure S1. The proton conductivity of BZY [1, 2] a), BCY [3] b) under high pressure, and $BaZr_{0.8-x}Ce_xY_{0.2}O_{3-\delta}$ (x=0, 0.1 and 0.2, denoted as BZCY0 to 20) with varying Ce content [4] c). Solid lines show the range that the activation energies and prefactors were extracted. Red circles indicate the point that the proton conductivities intersect.

Raman peak analysis

1. Baseline subtraction

An iterative polynomial algorithm was used to fit the baselines of each Raman spectra in this work and the baseline was subtracted, thereof. A fifth-order of polynomial was used in the fitting procedures.[5] Spectral region from 100 cm^{-1} to 1000 cm^{-1} of the spectra was processed.

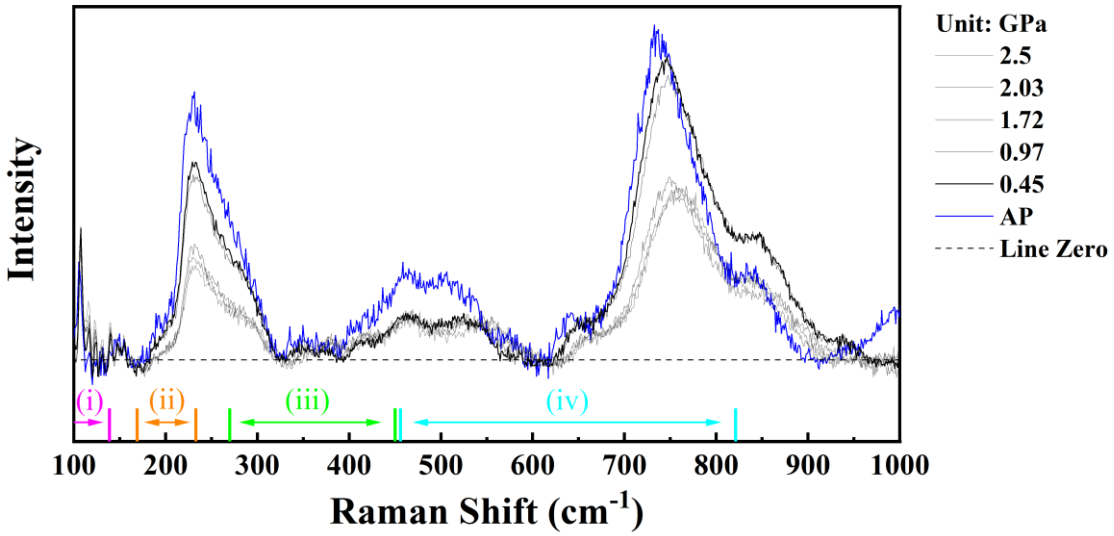

Figure S2. Pressure-dependent Raman spectra (after baseline subtraction) for BZY. (i) Ba-ZrO_6 stretching, (ii) ZrO_6 torsion, (iii) O-Zr-O bending, (iv) Zr-O stretching.

2. Multi-peak fitting

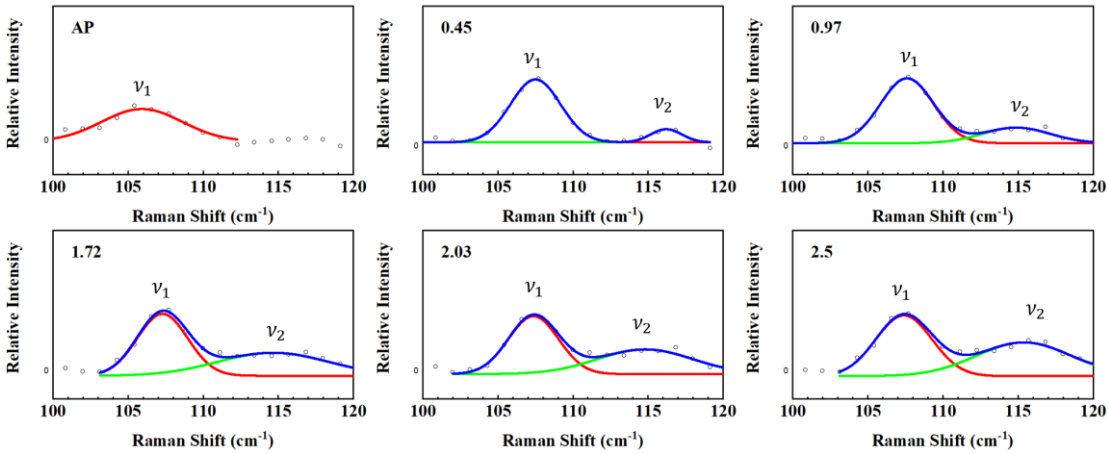

Figure S3. Raman peak fitting diagram from ambient pressure (AP) to 2.5 GPa for the Ba-ZrO_6 stretching motion of BZY from 100 to 150 cm^{-1}. Black open circles: experimental data; blue line: cumulative fit for the Raman peak; red line: ν_1; green line: ν_2. Two Gaussian functions were used in the peak fitting procedure.

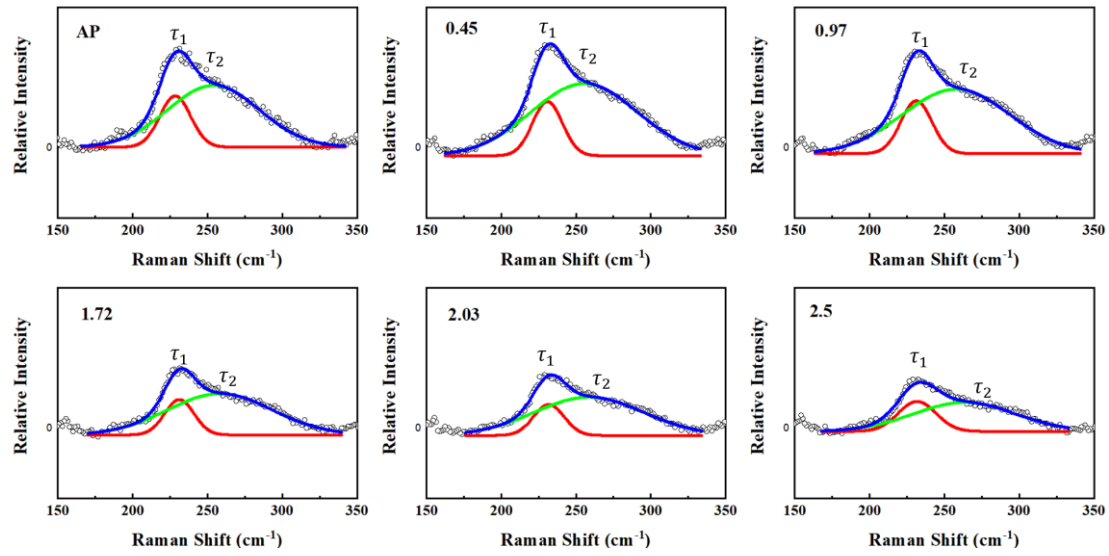

Figure S4. Raman peak fitting diagram from AP to 2.5 GPa for the ZrO_6 torsional motion of BZY from 200 to 350 cm^{-1}. Black open circles: experimental data; blue line: cumulative fit; red line: τ_1; green line: τ_2. Two Gaussian functions were used in the peak fitting procedure.

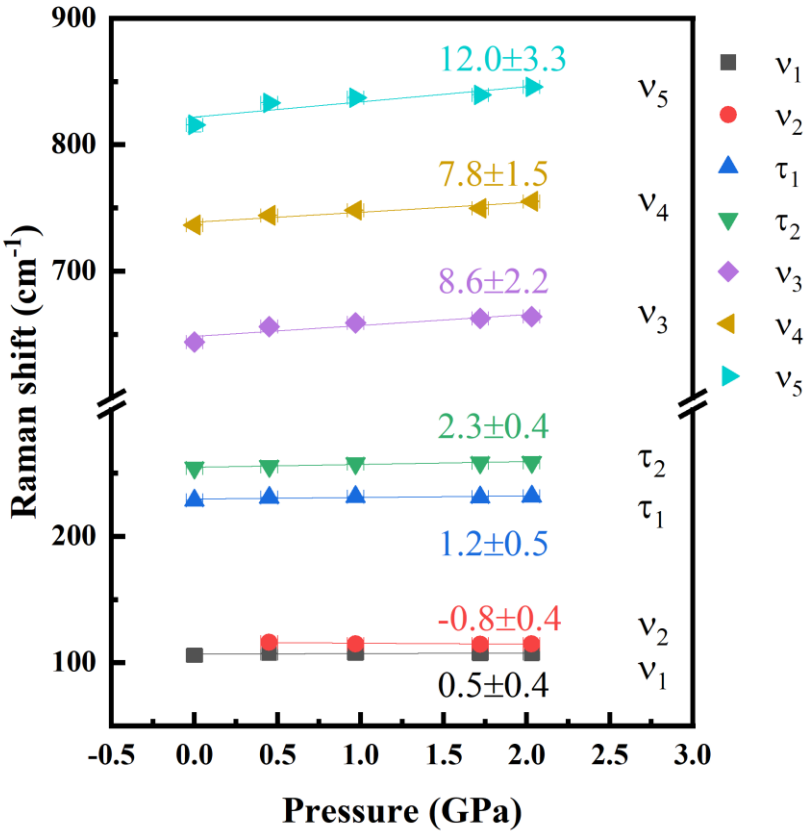

Figure S5. Raman shift of the vibrational modes in BZY as a function of pressure. Error bars are within the size of symbols.

Evolution of lattice parameters under pressure

According to the XRD structural refinement in Figure S6a, we obtained the pressure-dependent lattice volume and the Zr-O bond length, as shown in Figure S6b. The Birch−Murnaghan equation of state was use to fit the pressure-volume (P-V) diagram, with the first-pressure derivative of the bulk modulus K'_0 taken as 4 [6]:

$$P = \frac{3K_0}{2}\left[\left(\frac{V}{V_0}\right)^{-\frac{7}{3}} - \left(\frac{V}{V_0}\right)^{-\frac{5}{3}}\right] \qquad (S1.)$$

where K_0 is the isothermal bulk modulus and, V_0 is the unit cell volume at ambient pressure. From the fit to the P−V curve, we obtain the bulk modulus K_0= 151.9 ± 24 GPa, and V_0 = 74.6 ± 0.12 Å^3. The relationship between Zr-O bond length and pressure was then determined.

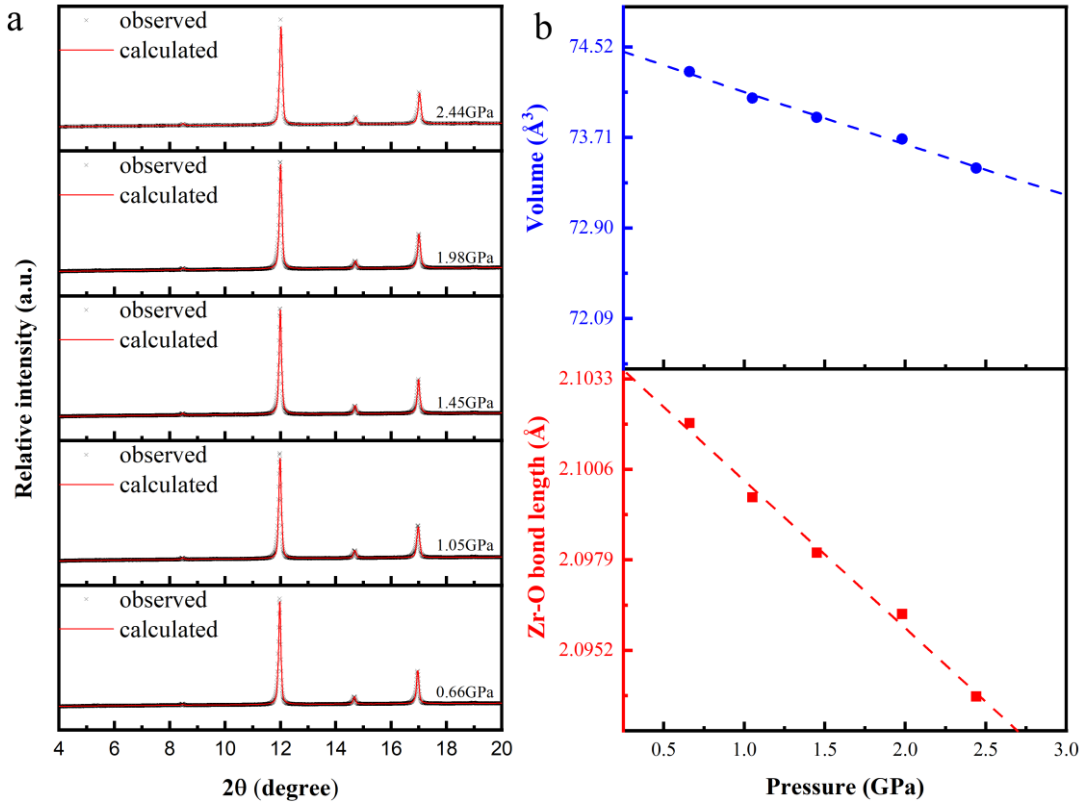

Figure S6. Pressure-dependent X-ray diffractogram for BZY: a) Structural refinement of XRD pattern from 0.66 to 2.44 GPa (with Rf-factor < 4%, Bragg R-factor < 5%); b) Upper: pressure−volume diagram of BZY, Lower: pressure-dependent Zr-O bond length. Dashed lines represent the fit according to the Birch−Murnaghan equation of state with $K'_0 = 4$.

Contribution of specific Raman modes

According to Fig. 3, E_a can be considered as a function of all the vibration modes, i.e. $E_a(\nu_1, \nu_2, \tau_1, \tau_2, \nu_3, \nu_4, \nu_5)$. Take partial differential of E_a over all the frequencies,

$$dEa = \left(\frac{\partial Ea}{\partial \nu_1}\right) d\nu_1 + \left(\frac{\partial Ea}{\partial \nu_2}\right) d\nu_2 + \left(\frac{\partial Ea}{\partial \tau_1}\right) d\tau_1 + \left(\frac{\partial Ea}{\partial \tau_2}\right) d\tau_2 + \left(\frac{\partial Ea}{\partial \nu_3}\right) d\nu_3 + \left(\frac{\partial Ea}{\partial \nu_4}\right) d\nu_4 + \left(\frac{\partial Ea}{\partial \nu_5}\right) d\nu_5$$

If we consider all the vibration modes were equally weighted, that is, all coefficients were approximately equal, e.g.

$$\left(\frac{\partial Ea}{\partial \nu_1}\right) \approx \left(\frac{\partial Ea}{\partial \nu_2}\right) \approx \left(\frac{\partial Ea}{\partial \tau_1}\right) \approx \left(\frac{\partial Ea}{\partial \tau_2}\right) \approx \left(\frac{\partial Ea}{\partial \nu_3}\right) \approx \left(\frac{\partial Ea}{\partial \nu_4}\right) \approx \left(\frac{\partial Ea}{\partial \nu_5}\right)$$

From Fig. 3, we can see that the changes in ν_3, ν_4, ν_5 ($d\nu_3$, $d\nu_4$ and $d\nu_5$) are much larger than the changes in the other vibration modes, suggesting that these modes contribute the most to changes in E_a.

Raman frequency for $BaZr_{0.8-x}Ce_xY_{0.2}O_{3-\delta}$ (x=0, 0.1 and 0.2)

$BaZr_{0.8}Y_{0.2}O_{3-\delta}$, $BaZr_{0.7}Ce_{0.1}Y_{0.2}O_{3-\delta}$ and $BaZr_{0.6}Ce_{0.1}Y_{0.2}O_{3-\delta}$ were prepared using the same method as $BaZr_{0.9}Y_{0.1}O_{3-\delta}$ described in this work. Raman Scattering spectra were collected with a Senterra R200-L Dispersive Confocal Raman Spectrometer using 10mW 532nm laser, a 50× magnification objective, and with the accumulation of 1s.

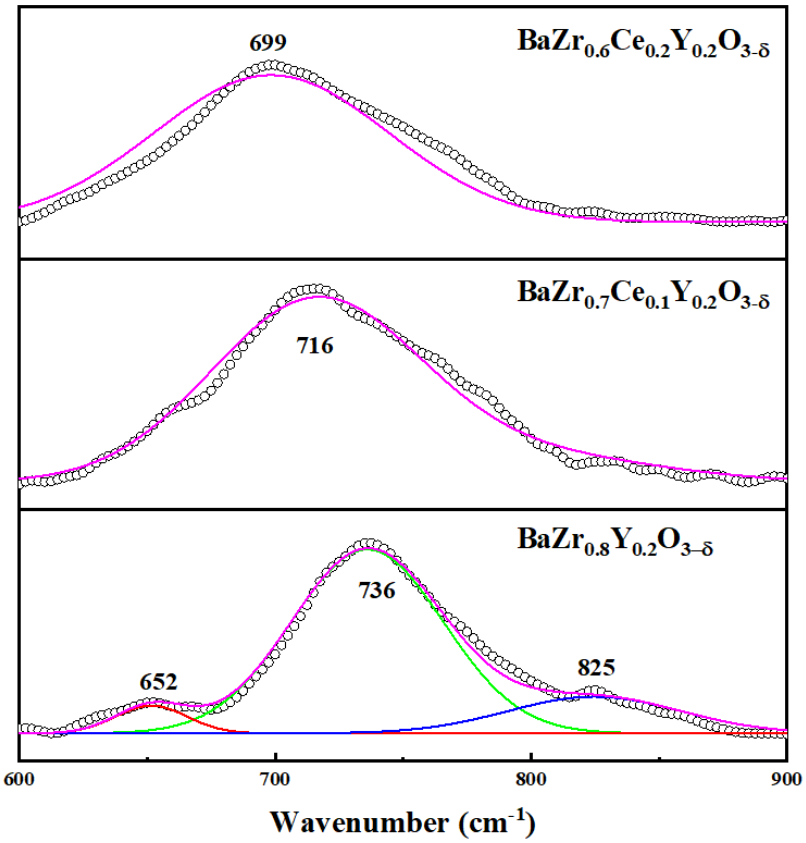

Figure S7. Raman peak fitting diagram from 600 to 900 cm^{-1} for $BaZr_{0.8}Y_{0.2}O_{3-\delta}$, $BaZr_{0.7}Ce_{0.1}Y_{0.2}O_{3-\delta}$ and $BaZr_{0.6}Ce_{0.1}Y_{0.2}O_{3-\delta}$. Black open circles: experimental data; purple line: cumulative fit; red line: v_3; green line: v_4; blue line: v_5. Three Gaussian function were used in the peak fitting procedure for $BaZr_{0.8}Y_{0.2}O_{3-\delta}$; for $BaZr_{0.7}Ce_{0.1}Y_{0.2}O_{3-\delta}$ and $BaZr_{0.6}Ce_{0.1}Y_{0.2}O_{3-\delta}$, the three bands merge into one, therefore one Gaussian function was used in fitting.

Enhancement of proton conductivity by tuning T_{iso}

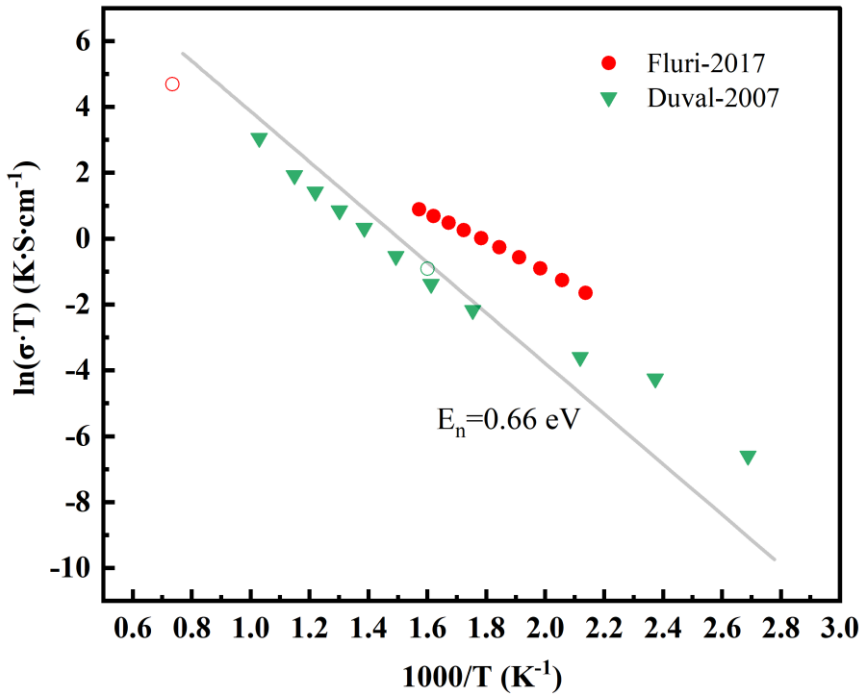

Figure S8. The bulk proton conductivity of $BaZr_{0.9}Y_{0.1}O_{3-\delta}$ (BZY10) reported in ref. [7] for sintered pellet and in ref. [8] with epitaxial strain, respectively. The green open circle shows the isokinetic-temperature of BZY10 reported in this work. The red open circle is the isokinetic temperature for BZY10 epitaxial film. The solid line indicates the critical energy determined by Equation (5).

References

[1] Q. Chen, A. Braun, A. Ovalle, C. D. Savaniu, T. Graule, N. Bagdassarov, Applied Physics Letters 2010, 97, 333.
[2] Q. Chen, Doctoral thesis, ETH Zurich No. 20554, 2012.
[3] Q. Chen, A. Braun, S. Yoon, N. Bagdassarov, T. Graule, Journal of the European Ceramic Society 2011, 31, 2657.
[4] D. Han, K. Goto, M. Majima, T. Uda, ChemSusChem 2021.
[5] J. Zhao, H. Lui, D. I. McLean, H. Zeng, Applied spectroscopy 2007, 61, 1225.
[6] Z. Fan, N. Li, P. Du, W. Yang, Q. Chen, The Journal of Physical Chemistry C 2020, 124, 22376.
[7] A. Fluri, A. Marcolongo, V. Roddatis, A. Wokaun, D. Pergolesi, N. Marzari, T. Lippert, Advanced Science 2017, 4, 1700467.
[8] S. Duval, P. Holtappels, U. Vogt, U. Stimming, T. Graule, Fuel Cells 2009, 9, 613.